Polarized laser-selective excitation and Zeeman infrared absorption of Sm^{3+} centers in CaF_2 and SrF_2 crystals

Jon-Paul R. Wells* and Roger J. Reeves
Department of Physics and Astronomy, University of Canterbury, PB4800, Christchurch, New Zealand
(Received 3 January 2000)

Laser-selective excitation and fluorescence and Zeeman infrared-absorption spectroscopy have been employed to study Sm^{3+} centers in doped CaF_2 and SrF_2 crystals. The dominant center present in both host crystals has been determined to consist of a C_{4v} symmetry Sm^{3+}-F^- pair. A weakly fluorescing, nonlocally charge-compensated Sm^{3+} ion center has also been observed. These centers have cubic symmetry. In CaF_2:Sm^{3+}, absorption features at 17 809 and 17 828 cm^{-1} yield no visible fluorescence upon resonant excitation. These transitions are associated with anion excess dimer and trimer centers of which the Sm^{3+} optical excitation is entirely quenched through nonradiative cross relaxation energy transfer. Codoping the crystals with La^{3+}, Ce^{3+}, Gd^{3+} or Tb^{3+} ions creates heterogeneous clusters from which Sm^{3+} fluorescence is observed. However, in the case of codoping with Eu^{3+}, efficient and complete $Sm^{3+}(^4G_{5/2})\rightarrow Eu^{3+}(^5D_0)$ energy transfer is observed through multi-phonon-assisted processes. Treating the crystals with oxygen yields C_{3v} symmetry centers associated with O^{2-} charge compensation. Crystal- and magnetic-field analyses of the O_h and C_{4v} symmetry centers gives optimized crystal-field parameters which are consistent with those of other rare-earth ions and which well account for the magnetic splitting measured by Zeeman infrared absorption.

I. INTRODUCTION

The alkaline-earth fluoride lattice consists of a body-centered-cubic structure. The F^- ions form a cubic cage with the alkaline-earth cation residing at the center of each alternate cage. Trivalent rare-earth ions (R^{3+}) readily substitute for the divalent alkaline-earth cation and charge compensation is required. In CaF_2:R^{3+} crystals, the well-known $C_{4v}(F^-)$ center is predominant. This center consists of a R^{3+}-F^- pair with the charge-compensating fluorine ion located in the nearest-neighbor position along the [100] direction from the R^{3+} ion.[1–8] SrF_2:R^{3+} is less simple with ions up to Dy^{3+} having a predominant $C_{4v}(F^-)$ center. Between Ho^{3+} and Er^{3+} a changeover from the tetragonal $C_{4v}(F^-)$ center to a predominant center of C_{3v} symmetry occurs.[6,9] This center consists of a R^{3+}-F^- pair with the charge compensating F^- ion located in the next-nearest-neighbor position along the [111] direction from the R^{3+} ion (the so-called *J* center).

Samarium often exists in mixed valence states when doped into alkaline-earth fluoride crystals due to the partial reduction of Sm^{3+} during the growth procedure. Divalent Sm^{2+} in CaF_2 and SrF_2 has been studied extensively (see, for example, Ref. 10). This interest was largely motivated by the success in obtaining laser action from the divalent species at 77 K (Refs. 11 and 12) and optical memory applications related to photoionization hole burning.

In contrast, trivalent Sm^{3+} in CaF_2 and SrF_2 has received little attention. Early electron paramagnetic resonance studies[13,14] found a dominant center of C_{4v} symmetry in CaF_2:Sm^{3+}. However, later studies in CaF_2:Sm^{3+} and SrF_2:Sm^{3+} (Refs. 15–17) found a consistent C_{4v} symmetry center that was spectroscopically distinct and thus differing in charge compensation configuration from the earlier studies. Several optical studies were undertaken. The first of these, by Ewanizky, Caplan, and Pastore[18] found a degraded polarization behavior for the C_{4v} center fluorescence. No definitive explanation for this was given. Later, Rabbiner[19] reanalyzed the data in terms of the electrostatic crystal-field experienced by the Sm^{3+} ion. However, the analysis has limitations due to the nonselectivity of the measurements upon which it was based. Nara and Schlesinger[20] also attempted crystal-field analyses, but, as with Rabbiner, the quality of the data precluded any serious analysis.

At high concentrations of rare-earth ions in CaF_2, multi-R^{3+} ion centers exist which are known to be anion excess.[21–23] For ions heavier than Gd^{3+}, it is predicted that hexamer clusters are the predominant form of defect clustering, as appears to have been observed in CaF_2:Er^{3+},[24–26] and in CaF_2:Lu^{3+} crystals codoped with Gd^{3+}.[27] Previous laser-selective excitation measurements of CaF_2:Eu^{3+} have identified two cluster centers.[4] The arbitrarily labeled *R* center is a negatively charged cluster which consists of two Eu^{3+} ions and three F^- ions distributed in such a manner that the two Eu^{3+} ions experience different site potentials. The remaining center, labeled *Q*, is a symmetric cluster of three Eu^{3+} ions with four F^- ions.[28,29] These clusters, well known for Eu^{3+}, are reported here for Sm^{3+} centers in CaF_2, having observable exchange splittings in their infrared-absorption lines. As the concentration of clusters increases, there is a corresponding increase in the population of cubic (nonlocally charge compensated) centers. This is found to occur through ''gettering'' of the F^- ions by the cluster centers by dissociation of the single R^{3+}-F^- dipoles.[30]

This paper presents optical and infrared spectroscopy of Sm^{3+} centers in CaF_2 and SrF_2 crystals. Polarized laser-excited fluorescence has been used to infer center symmetries and establish comprehensive energy-level schemes for a total of 16 different rare-earth ion centers. Extremely efficient $Sm^{3+}(^4G_{5/2})\rightarrow Eu^{3+}(^5D_0)$ energy transfer has been

observed in CaF_2:0.15% Eu^{3+}:0.05% Sm^{3+}. Single-electron crystal-field analyses have been performed for the O_h and C_{4v} symmetry centers in both CaF_2 and SrF_2 which yield optimized parameters consistent with those observed for other rare-earth ions. The calculated crystal-field wave functions give a good account of the magnetic splitting factors measured by Zeeman infrared absorption.

II. EXPERIMENTAL TECHNIQUES

For all spectroscopic studies undertaken here, CaF_2 and SrF_2 crystals containing the appropriate quantity of SmF_3 were grown by the Bridgman-Stockbarger method at the University of Canterbury. The starting materials were placed in a graphite crucible and lowered at 4 mm h^{-1} through the temperature gradient produced by the induction coil of a 38-kW rf furnace. Oriented samples for polarization studies were cut from boules aligned using the (111) cleavage planes. All of the Sm^{3+}-doped CaF_2 and SrF_2 samples used in this study were completely clear, indicating the absence of the divalent species. In all cases, PbF_2 was added to the start material to scavenge for unintentional oxygen impurities. For intentional oxygen implantation, a variant on the method of Hall and Schumacher[31] for the introduction of hydrogen and deuterium into fluorite crystals was used. This involved the heating of the samples to be treated, in dry oxygen gas at 850 °C for periods ranging between 15 min to 4 h.

Optical-absorption spectra showing transitions to the $^4G_{5/2}$ multiplet of the Sm^{3+} ion were recorded on a Spex 1700 0.75-m monochromator using an EMI 9659 QA photomultiplier. Electromagnetic radiation was provided by a voltage-stabilized 100-W quartz iodine lamp. Spectra were recorded at temperatures down to 16 K using a CTI-Cryogenics model 22C cryodyne cryocooler.

Laser excitation was provided by a Spectra-Physics 375 dye laser pumped by a Spectra-Physics model 2045E 15-W argon laser. The resulting fluorescence was detected by a Spex 1403 double monochromator with a thermoelectrically cooled RCA C31034A photomultiplier using photon-counting techniques. Either Rhodamine 560 or Coumarin 540 dyes were appropriate for excitation of $^4G_{5/2}$ (Coumarin 540 can also excite the $^4F_{3/2}$ multiplet at 18 900 cm^{-1}). For long-wavelength fluorescence to the ^6F_J multiplets, an RCA 7102 photomultiplier cooled to −100 °C in a Products for Research model TE 176-RF liquid nitrogen refrigeration chamber, was used to detect fluorescence on the Spex 1700 single monochromator.

Fluorescence lifetimes were recorded using a Photochemical Research Associates (PRA) model LN1000 nitrogen laser to excite a PRA model LN107 dye laser. The nitrogen laser has an output energy of up to 110 the μJ per pulse. A Spex 1700 single monochromator with an EMI 9659 QA photomultiplier (PMT) was used to detect emission. The PMT signal was amplified and stored on a Hitachi model VC6275 digital storage oscilloscope.

Infrared absorption spectra were measured with 0.1 cm^{-1}-resolution on a BioRad FTS-40 Fourier Transform infrared spectrometer. The crystal samples were mounted on a copper holder and cooled by thermal contact with the 10-K stage of a CTS LTS 0.1 closed-cycle helium cryostat. Zeeman spectra were measured with a 4-T Oxford Instruments superconducting solenoid built into the can of a liquid-helium cryostat. The infrared beam was directed along a hollow tube fixed through the center of the solenoid. The crystals were cooled by thermal contact with a copper sample holder screwed into the middle of this tube. As the magnet is a simple solenoid, Zeeman infrared measurements could only be made with the radiation beam along the direction of the magnetic field, which restricted observations to allowed transitions for the $\mathbf{B}\|\mathbf{k}$ polarization geometry.

III. SPECTROSCOPY OF Sm^{3+} IN CaF_2 AND SrF_2

A. Energy levels of Sm^{3+} ions in centers of O_h, C_{4v}, and C_{3v} symmetry

The $4f^5$ configuration is appropriate for trivalent samarium and consists of 1001 two fold (Kramers) degenerate electronic states. Two multiplets ($^4G_{5/2}$ at 17 800 cm^{-1} and $^4F_{3/2}$ at 18 900 cm^{-1}) are accessible to Coumarin 540 dye laser excitation. The ground multiplet is $^6H_{5/2}$, and fluorescence to all multiplets of the low lying ^6H_J and ^6F_J terms (except $^6F_{9/2}$ and $^6F_{11/2}$) could be detected with the photomultipliers used in this study.

The standard notation of a letter plus a numerical subscript is used here for labeling the crystal-field levels of various LSJ multiplets. The ground multiplet is labeled Z, with the ground state being Z_1, and the first excited multiplet $^6H_{7/2}$ labeled by Y. The levels of the $^4G_{5/2}$ multiplet are lebeled A_1, A_2, and A_3 while the levels of $^4F_{3/2}$ are denoted B_1 and B_2.

All of the Sm^{3+} energy levels have wave functions which necessarily transform as one of the irreducible representations (irreps) of the appropriate double group describing the symmetry of the local crystal environment around the ion. For Sm^{3+} ions in centers of cubic symmetry, the energy levels transform as one of the double dimensional $^{(2)}\Gamma_6$ and $^{(2)}\Gamma_7$ irreps, or the fourfold dimensional $^{(4)}\Gamma_8$ irrep of the O_h double group. For Sm^{3+} ions in centers of C_{4v} symmetry, the energy levels transform as either the γ_6 or γ_7 irreps of the C_{4v} double group, while Sm^{3+} ions in centers of trigonal symmetry transform as either the γ_4 or $\gamma_{5,6}$ C_{3v} double-group irreps.

The polarization behavior of Kramers ions in C_{4v} and C_{3v} symmetry centers was presented by Cockcroft *et al.*[7] for the case of emission of electric dipole character. When considering emission of magnetic dipole character, the transverse oscillation of the magnetic vector of the propagating electromagnetic wave gives rise to inverted polarization ratios. Obviously, the absorption and emission features of Sm^{3+} ions in centers of O_h symmetry do not display any intensity dependence upon either the orientation of the crystal or the polarization of the exciting laser beam.

B. Absorption, laser-selective excitation, and fluorescence spectra

Measurement of absorption gives the clearest picture of the defect center distribution in a R^{3+} activated crystal. In an absorption measurement, there is no need to correct for the differing quantum efficiencies of a R^{3+} ion in a given center. In this case, we detect the $^6H_{5/2}\rightarrow{}^4G_{5/2}$ absorption transitions of the Sm^{3+} ion centered around 17 800 cm^{-1}. These transi-

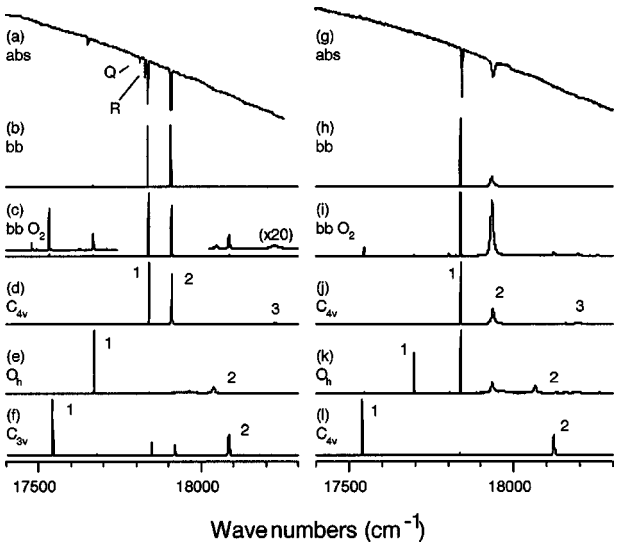

FIG. 1. (a) and (g) 16-K, $^4G_{5/2}$ optical-absorption spectra for CaF_2:0.05% Sm^{3+} and SrF_2:0.05% Sm^{3+} respectively. (b) and (h) 16-K, $^4G_{5/2}$ laser excitation spectra monitoring all fluorescence in zero order of diffraction for CaF_2:0.05% Sm^{3+} and SrF_2:0.05% Sm^{3+}. (c) and (i) 16-K, $^4G_{5/2}$ laser excitation spectra monitoring all fluorescence in zero order of diffraction for CaF_2:0.05% Sm^{3+} and SrF_2:0.05% Sm^{3+} crystals which have been oxygenated for 30 min. Laser-selective excitation spectra (d) for the $C_{4v}(F^-)$ center (monitoring at 14 333 cm^{-1}), (e) for the O_h center (monitoring at 12 804 cm^{-1}) and (f) for the $C_{3v}(O^{2-})$ center (monitoring at 13 900 cm^{-1}) in CaF_2:0.05% Sm^{3+}. Laser-selective excitation spectra (j) for the $C_{4v}(F^-)$ center (monitoring at 16 731 cm^{-1}), (k) for the O_h center (monitoring at 16 606 cm^{-1}) and (l) for the $C_{3v}(O^{2-})$ center (monitoring at 16 575 cm^{-1}) in SrF_2:0.05%Sm^{3+}.

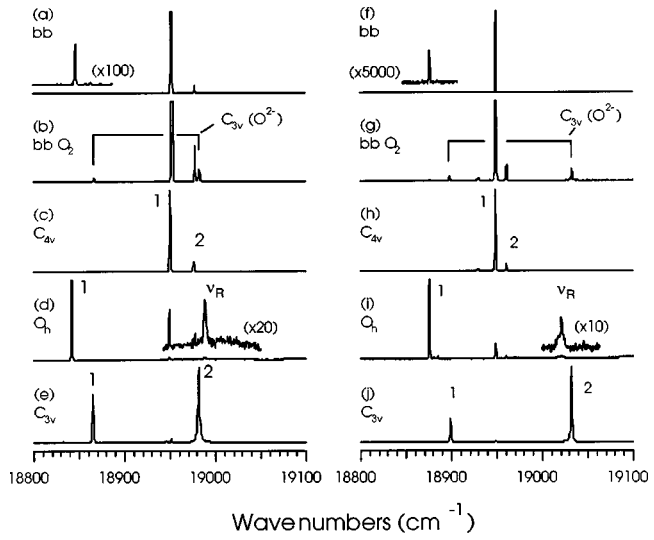

FIG. 2. (a) and (f) 16-K, $^4F_{3/2}$ laser excitation spectra monitoring all fluorescence in zero order of diffraction for CaF_2:0.05% Sm^{3+} and SrF_2:0.05% Sm^{3+}. (b) and (g) 16-K, $^4F_{3/2}$ laser excitation spectra monitoring all fluorescence in zero order of diffraction for CaF_2:0.05% Sm^{3+} and SrF_2:0.05% Sm^{3+} crystals oxygenated for 30 min. Laser-selective excitation spectra (c) for the $C_{4v}(F^-)$ center (monitoring at 17 837 cm^{-1}), (d) for the O_h center (monitoring at 17 653 cm^{-1}) and (e) for the $C_{3v}(O^{2-})$ center (monitoring at 17 511 cm^{-1}) in CaF_2:0.05% Sm^{3+}. Laser-selective excitation spectra (h) for the $C_{4v}(F^-)$ center (monitoring at 17 839 cm^{-1}), (i) for the O_h center (monitoring at 17 699 cm^{-1}), and (j) for the $C_{3v}(O^{2-})$ center (monitoring at 17 544 cm^{-1}) in SrF_2:0.05% Sm^{3+}. ν_R denotes a cubic center resonance vibration.

tions are nominally spin forbidden, but this selection rule is broken down via intermediate coupling, and transitions are observed at around five percent of the total transmission through the crystal.

Figure 1(a) shows the $^6H_{5/2} \rightarrow {}^4G_{5/2}$ absorption spectra of CaF_2:0.05% Sm^{3+} using an optical path length of 20 mm. Five absorption transitions are readily apparent at frequencies of 17 653, 17 809, 17 828, 17 837, and 17 908 cm^{-1}. Comparison of this spectrum with laser excitation (fluorescence detected absorption) spectra employing both broadband and frequency-selective detection [shown in Figs. 1(b), 1(d), and 1(e)] shows that there are two discrete fluorescing centers. The two dominant peaks in both the absorption and excitation spectra, at 17 837 and 17 908 cm^{-1}, are associated with the expected $C_{4v}(F^-)$ symmetry center as determined from the polarization behavior of the fluorescence transitions. The 17 653-cm^{-1} feature is a cubic center transition. The observation of transitions corresponding to a cubic cen-

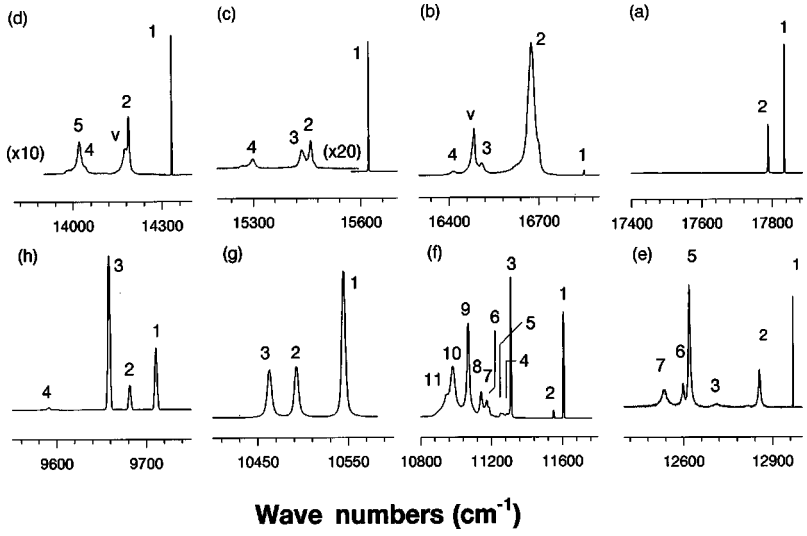

FIG. 3. 16-K unpolarized fluorescence spectra for the (a) $^6H_{5/2}$, (b) $^6H_{7/2}$, (c) $^6H_{9/2}$, (d) $^6H_{11/2}$, (e) $^6H_{13/2}$, (f) $^6H_{15/2}$, $^6F_{1/2}$, and $^6F_{3/2}$, (g) $^6F_{5/2}$, and (h) $^6F_{7/2}$ multiplets of the $C_{4v}(F^-)$ center in CaF_2:0.05% Sm^{3+} crystals. v denotes a transition terminating on a vibronic level.

TABLE I. 16-K calculated and experimental energy levels, and the (111) magnetic splitting factors of the $C_{4v}(F^-)$ center in $CaF_2:Sm^{3+}$ and $SrF_2:Sm^{3+}$. The energy levels are as measured in air (± 1 cm^{-1}) and the magnetic splitting factors are for an applied field of 4 T (except for levels of the $^6H_{7/5}$, $^6H_{7/2}$, and $^6H_{11/2}$ multiplets, which are at 3 T). The uncertainty on the measured splitting factors is ± 0.2 unless otherwise stated. The levels denoted † are from infrared absorption spectra. The splitting factors that are denoted *a* have been calculated assuming a first order Zeeman interaction only (see the text).

		$CaF_2:Sm^{3+}$				$SrF_2:Sm^{3+}$			
	State	Energy		$s_{(111)}$		Energy		$s_{(111)}$	
Multiplet	and Symmetry	Calc	Expt	Calc	Expt	Calc	Expt	Calc	Expt
$^6H_{5/2}$	$Z_1(\gamma_6)$	10	0	0.8	0.6	7	0	0.8	0.7
	$Z_2(\gamma_7)$	50	47	0.8	-	33	35	0.2	-
	$Z_3(\gamma_7)$	366	-	0.6	-	259	-	0.7	-
$^6H_{7/2}$	$Y_1(\gamma_6)$	984	985	2.4	1.5	992	990	2.3	2.1
	$Y_2(\gamma_7)$	1169	1160	3.1	-	1113	1108	3.1	-
	$Y_3(\gamma_7)$	1334	1323	1.8	-	1276	1283	1.8	-
	$Y_4(\gamma_6)$	1402	1418	3.2	-	1300	1309	3.0	-
$^6H_{9/2}$	$X_1(\gamma_6)$	2208	2215	3.8	3.8	2212	2216	3.8	3.7
	$X_2(\gamma_6)$	2375	2376	4.2	4.4	2324	2330	4.3	4.5 ± 0.4
	$X_3(\gamma_7)$	2393	2403	3.7	-	2342	2345	3.9	-
	$X_4(\gamma_7)$	2530	2537	3.9	-	2477	2486	3.9	-
	$X_5(\gamma_6)$	2627	-	5.2	-	2519	2527	5.1	-
$^6H_{11/2}$	$W_1(\gamma_6)$	3496	3504	5.1	4.9	3510	3513	5.0	4.8
	$W_2(\gamma_7)$	3653	3648	3.0	-	3621	3619	3.3	-
	$W_3(\gamma_6)$	3740	-	5.7	-	3688	-	5.6	-
	$W_4(\gamma_5)$	3792	3795	4.7	-	3740	3745	4.7	-
	$W_5(\gamma_7)$	3809	3814	3.0	-	3756	3760	2.6	-
	$W_6(\gamma_7)$	3975	-	6.5	-	3863	3824	6.0	-
$^6H_{13/2}$	$V_1(\gamma_6)$	4859	4866	7.0	6.9	4881	4885	7.0	6.8
	$V_2(\gamma_7)$	4976	4981	2.6	-	4969	4871	3.2	1.8
	$V_3(\gamma_7)$	5131	5125	4.0	-	5092	5078	5.0	-
	$V_4(\gamma_6)$	5215	-	2.8	-	5157 (γ_7)	5154	6.2	6.4 ± 0.3
	$V_5(\gamma_7)$	5216	5217	1.6	-	5167 (γ_6)	5181	4.8	-
	$V_6(\gamma_6)$	5240	5238	6.1	-	5189	5198	6.1	-
	$V_7(\gamma_7)$	5320	5300	8.6	-	5208	5210	7.7	-
$^6H_{15/2}$, $^6F_{1/2}$ and $^6F_{3/2}$	$S_1(\gamma_7)$	6231	6230	7.7	7.7	6246	6241	7.4	7.4
	$S_2(\gamma_6)$	6281	6286	6.5	6.4	6281	6282	6.4	6.5
	$S_3(\gamma_6)$	6549	6527	1.8	2.4 ± 0.3	6487	6466	3.8	3.7 ± 0.3
	$S_4(\gamma_6)$	6583	6580	3.7	-	6521	6500	6.0	-
	$S_5(\gamma_7)$	6847	6651	7.5	-	6596 (γ_6)	6619	5.3	6.5 ± 0.5
	$S_6(\gamma_6)$	6667	6660	4.8	-	6640 (γ_7)	6636	7.2	-
	$S_7(\gamma_6)$	6692	6693	4.8	-	6655 (γ_7)	6650	5.7	6.6 ± 0.5
	$S_8(\gamma_7)$	6766	6768	5.1	-	6701	6702	5.5	-
	$S_9(\gamma_6)$	6859	6852	3.9	-	6787	6787	4.7	-
	$S_{10}(\gamma_7)$	6878	6885	3.3	-	6796 (γ_6)	-	4.1	-
	$S_{11}(\gamma_7)$	6916	-	6.9	-	6812	-	3.2	-
$^6F_{5/2}$	$R_1(\gamma_7)$	7282	7293	1.9	1.2 ± 0.5	7220	7228	2.0	1.3 ± 0.3
	$R_2(\gamma_6)$	7340	7345	3.6	2.9 ± 0.5	7274	7274	3.6	2.8 ± 0.3
	$R_3(\gamma_7)$	7381	7375	3.8	3.8 ± 0.5	7311	7299	3.7	3.9 ± 0.3
$^6F_{7/2}$	$Q_1(\gamma_7)$	8130	8126	2.6	3.5	8076	8075	2.9	3.2
	$Q_2(\gamma_6)$	8151	8156	3.8	4.4	8094	8096	3.3	4.0
	$Q_3(\gamma_7)$	8156	8178	4.1	4.3	8103	8112	3.7	4.1
	$Q_4(\gamma_6)$	8250	8246	3.2	4.2 ± 0.5	8185	8173	3.1	3.9 ± 0.3

TABLE I. (*Continued*).

		$CaF_2:Sm^{3+}$				$SrF_2:Sm^{3+}$			
	State	Energy		$s_{(111)}$		Energy		$s_{(111)}$	
Multiplet	and Symmetry	Calc	Expt	Calc	Expt	Calc	Expt	Calc	Expt
$^6F_{9/2}$	$P_1(\gamma_6)$	9284	9269.9†	6.2[a]	6.0	9240	9234.2†	4.6	5.2
	$P_2(\gamma_6)$	9286	9288.4†	5.9[a]	5.3	9250	9244.0†	4.8	5.1
	$P_3(\gamma_7)$	9339	9356.4†	5.4	5.4	9277	9294.5†	5.3	4.9
	$P_4(\gamma_6)$	9359	9372.3†	4.9	4.5 ± 0.5	9299	9310.0†	4.3	4.1 ± 0.3
	$P_5(\gamma_7)$	9410	-	5.3	-	9346	9345.7†	5.3	-
$^6F_{11/2}$	$O_1(\gamma_7)$	10 585	-	9.2	-	10 577	-	9.1	-
	$O_2(\gamma_6)$	10 702	10 696.6†	4.6	-	10 647	10 653.5†	8.2	-
	$O_3(\gamma_7)$	10 712	-	5.4	-	10 650	10 669.4†	8.7	-
	$O_4(\gamma_6)$	10 730	10 733.7†	3.2	-	10 683	10 672.9†	5.3	-
	$O_5(\gamma_6)$	10 785	10 767.4†	5.7	-	10 730	10 704.8†	5.7	-
	$O_6(\gamma_7)$	10 794	-	6.4	-	10 735	-	6.1	-
$^4G_{5/2}$	$A_1(\gamma_7)$	17 538	17 837	1.5	-	17 831	17 839	1.4	-
	$A_2(\gamma_6)$	17 927	17 908	2.1	-	17 962	17 934	2.0	-
	$A_3(\gamma_7)$	18 219	18 240	2.2	-	18 175	18 195	2.0	-
$^4F_{3/2}$	$B_1(\gamma_6)$	18 944	18 950	0.8	-	18 943	18 949	0.7	-
	$B_2(\gamma_7)$	18 983	18 976	0.9	-	18 969	18 963	0.8	-

ter is not unexpected as the magnetic dipole transition moment is nonzero between states for which $\Delta J=0$ or ±1. Nonlocally charge-compensated R^{3+} centers have been observed previously in fluorite-type crystals, and are well documented.[32,33]

Two peaks in the absorption spectrum [Fig. 1(a)], at 17 809 and 17 828 cm^{-1}, are associated with nonfluorescing Sm^{3+} ion centers. These transition are labeled *Q* and *R*, respectively. Analogous *Q* and *R* centers have been previously observed in $CaF_2:Eu^{3+}$,[4] and have been assigned as trimer and dimer centers, respectively.[28,29,34] For these $CaF_2:Sm^{3+}$ analogs, the optical excitation of the Sm^{3+} ion can be quenched by cross-relaxation processes.[35]

By contrast, the $^6H_{5/2}\rightarrow{}^4G_{5/2}$ absorption spectrum of a 20-mm-thick SrF_2:0.05%Sm^{3+} crystal is simpler with only two features at 17 839 and 17 934 cm^{-1} which are analogous to those in $CaF_2:Sm^{3+}$ [see Fig. 1(g)]. The $^4G_{5/2}$ broadband and selective excitation spectra, which are shown in Figs 1(b) and 1(i), indicate that these transitions are associated with a $C_{4v}(F^-)$ center. In addition, a weaker cubic symmetry center is present. The selective excitation spectrum for this center is shown in Fig. 1(k).

Figures 2(a), 2(c), 2(d), 2(f), 2(h), and 2(j) show the $^4F_{3/2}$ excitation spectra, which display similar defect distributions as observed for $^4G_{5/2}$. The measured levels for the $^4G_{5/2}$ and $^4F_{3/2}$ multiplets in $CaF_2:Sm^{3+}$ and $SrF_2:Sm^{3+}$ are given in Tables I and II. In the $^4F_{3/2}$ excitation spectra, sharp cubic center vibronic transitions can be observed with energies of 139 and 150 cm^{-1} for the CaF_2 and SrF_2 hosts, respectively.[36] These are labeled with the notation ν_R. After

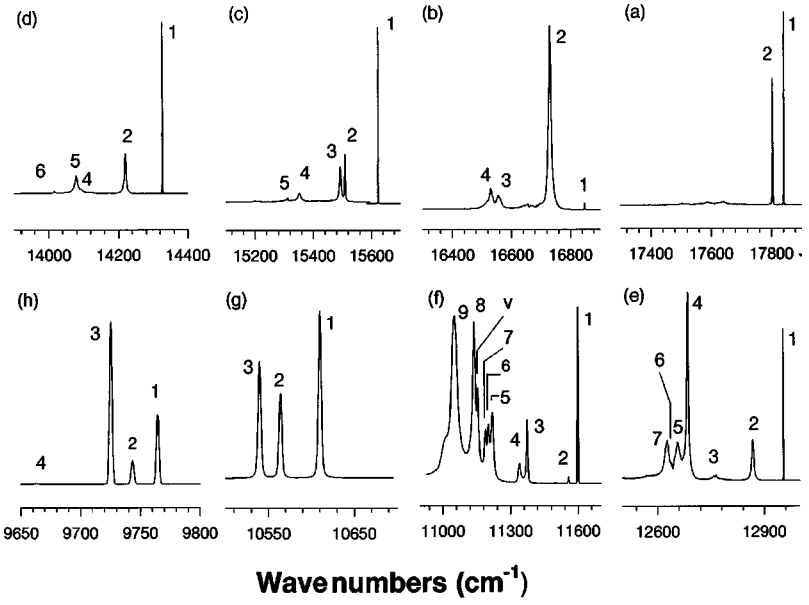

FIG. 4. 16-K unpolarized fluorescence spectra for the (a) $^6H_{5/2}$, (b) $^6H_{7/2}$, (c) $^6H_{9/2}$, (d) $^6H_{11/2}$, (e) $^6H_{13/2}$, (f) $^6H_{15/2}$, $^6F_{1/2}$, and $^6F_{3/2}$, (g) $^6F_{5/2}$, and (h) $^6F_{7/2}$ multiplets of the $C_{4v}(F^-)$ center in SrF_2:0.05% Sm^{3+} crystals. v denotes a transition terminating on a vibronic level.

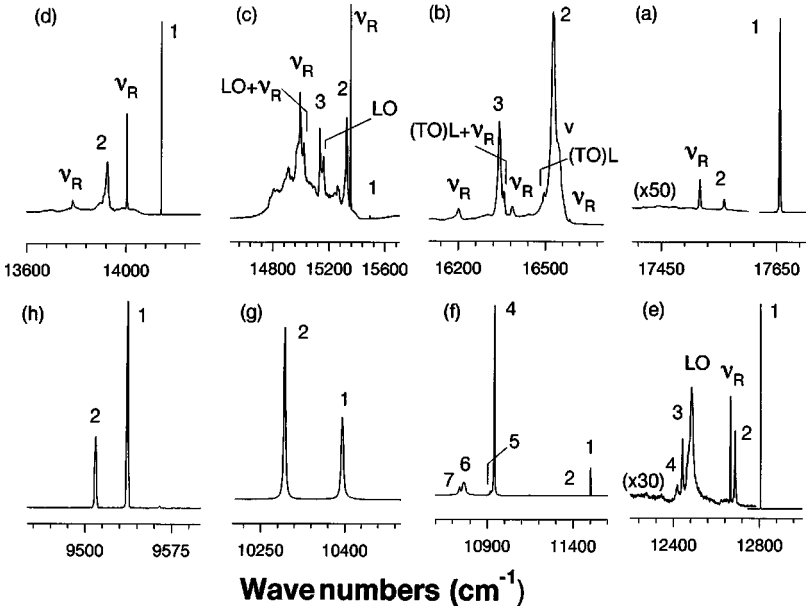

FIG. 5. 16-K unpolarized fluorescence spectra for the (a) $^6H_{5/2}$, (b) $^6H_{7/2}$, (c) $^6H_{9/2}$, (d) $^6H_{11/2}$, (e) $^6H_{13/2}$, (f) $^6H_{15/2}$, $^6F_{1/2}$, and $^6F_{3/2}$, (g) $^6F_{5/2}$, and (h) $^6F_{7/2}$ multiplets for the O_h center in CaF_2:0.05% Sm^{3+}. ν_R denotes a cubic center resonance vibration.

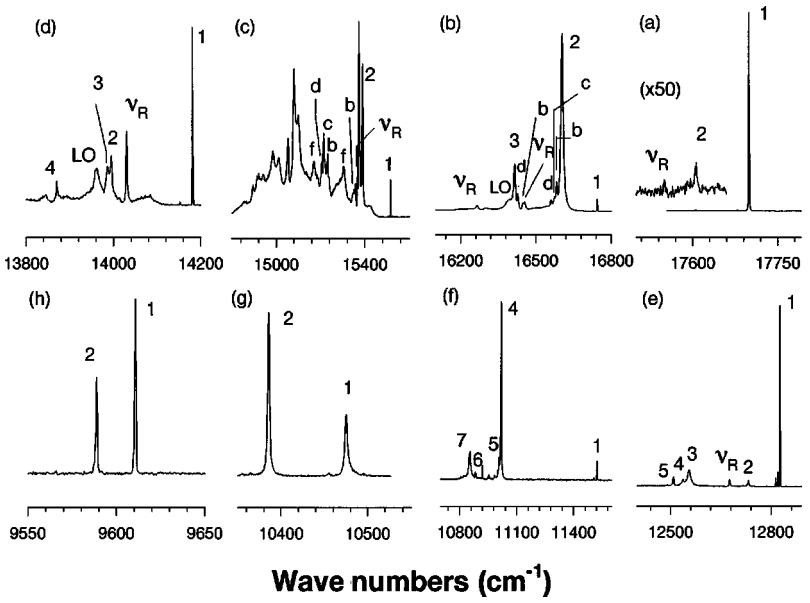

FIG. 6. 16-K unpolarized fluorescence spectra for the (a) $^6H_{5/2}$, (b) $^6H_{7/2}$, (c) $^6H_{9/2}$, (d) $^6H_{11/2}$, (e) $^6H_{13/2}$, (f) $^6H_{15/2}$, $^6F_{1/2}$, and $^6F_{3/2}$, (g) $^6F_{5/2}$, and (h) $^6F_{7/2}$ multiplets for the O_h center in SrF_2:0.05% Sm^{3+}. ν_R denotes a cubic center resonance vibration.

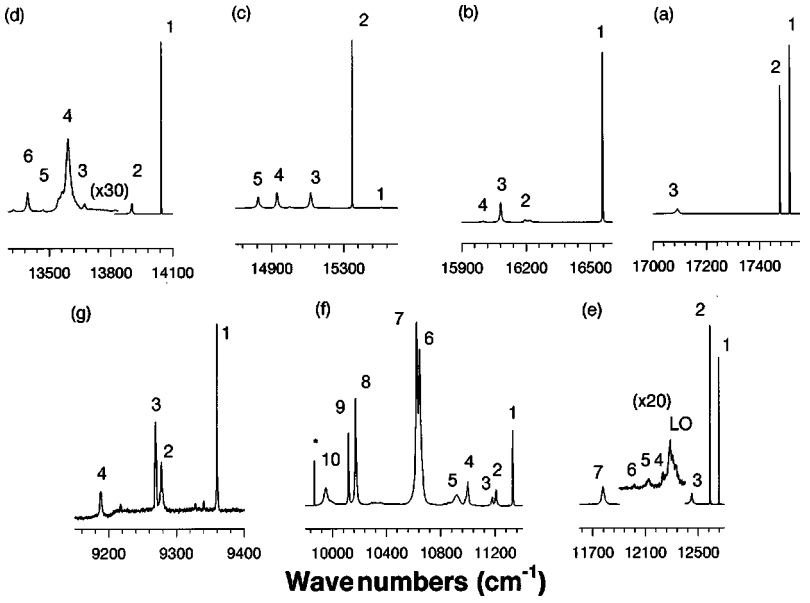

FIG. 7. 16-K unpolarized fluorescence spectra for the (a) $^6H_{5/2}$, (b) $^6H_{7/2}$, (c) $^6H_{9/2}$, (d) $^6H_{11/2}$, (e) $^6H_{13/2}$, (f) $^6H_{15/2}$, $^6F_{1/2}$, $^6F_{3/2}$, and $^6F_{5/2}$, and (g) $^6F_{7/2}$, multiplets of the $C_{3v}(O^{2-})$ center in oxygenated CaF_2:0.05% Sm^{3+} crystals. The * notation indicates an unassigned transition.

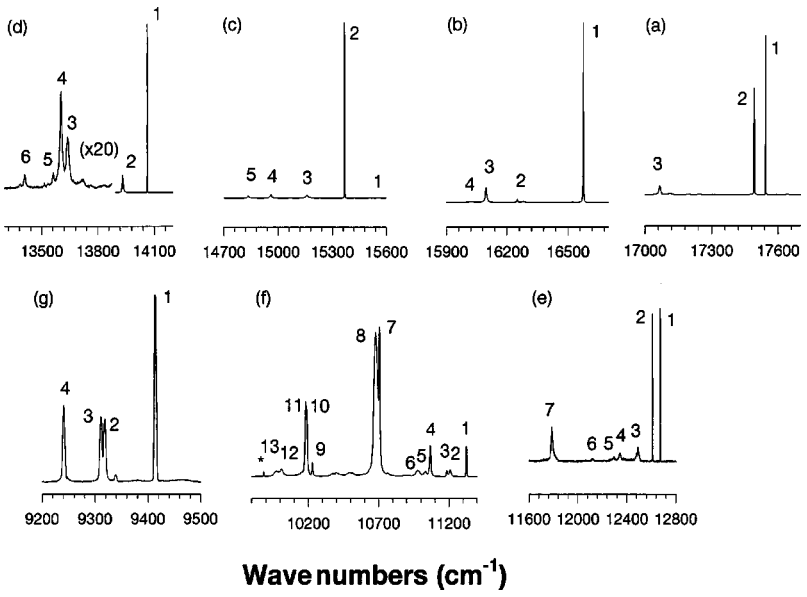

FIG. 8. 16-K unpolarized fluorescence spectra for the (a) $^6H_{5/2}$, (b) $^6H_{7/2}$, (c) $^6H_{9/2}$, (d) $^6H_{11/2}$, (e) $^6H_{13/2}$, (f) $^6H_{15/2}$, $^6F_{1/2}$, $^6F_{3/2}$, and $^6F_{5/2}$, and (g) $^6F_{7/2}$ multiplets of the $C_{3v}(O^{2-})$ center in oxygenated SrF_2:0.05% Sm^{3+} crystals. The * notation indicates an unassigned transition.

30 minutes treatment of both CaF_2:0.05% Sm^{3+} and SrF_2:0.05% Sm^{3+} in a dry oxygen atmosphere, a single center associated with O^{2-} charge compensation becomes apparent. The 17 511-cm^{-1} excitation peak was observed previously in CaF_2:Sm^{3+} crystals which were treated with oxygen.[25] The spectral character of this center is considerably different from the regular C_{4v} centers by having a much larger axial distortion. This is a feature consistent with the placement of an O^{2-} ion in the nearest-neighbor position along the [111] direction from the rare-earth ion, thus providing a center with C_{3v} symmetry. We denote this center as $C_{3v}(O^{2-})$. Figures 1(c), 1(f), 1(i), and 1(l) and 2(b), 2(e), 2(g), and 2(j) give the appropriate $^4G_{5/2}$ and $^4F_{3/2}$ broadband and selective excitation spectra.

1. $C_{4v}(F^-)$ center in CaF_2:0.05% Sm^{3+} and SrF_2:0.05% Sm^{3+} crystals

Absorption and laser excitation spectra of the $^4G_{5/2}$ and $^4F_{3/2}$ multiplets indicate that the dominant center in both CaF_2 and SrF_2 crystals is the $C_{4v}(F^-)$ center. This is confirmed by polarization studies of the $C_{4v}(F^-)$ center fluorescence. In (100)-oriented crystals, polarization ratios of 2:1 are obtained in a geometry consistent with a Kramers ion in a tetragonal C_{4v} symmetry center and the $^6H_{5/2}\rightarrow{}^4G_{5/2}$ pump transitions being magnetic dipole in character.[7] This is not unexpected given the magnetic dipole selection rule, $\Delta J = 0, \pm 1$.

Fluorescence to the $^6H_{5/2}$ multiplet (Figs. 3 and 4) was recorded for excitation of the $^4G_{5/2}A_3$ state, while for recording the fluorescence spectra of the remaining ^6H_J and accessible ^6F_J multiplets, the $Z_1\rightarrow A_1$ transition was excited. As observed previously,[18] the polarization dependence of the $C_{4v}(F^-)$ center fluorescence is degraded from the optimum ratio expected. This arises from the lack of a pure electric or magnetic dipole moment for the $^4G_{5/2}\rightarrow{}^6H_J$ and ^6F_J transitions. A magnetic dipole intensity is obtained because of J mixing between the relevant states through the crystal-field interaction. The measured crystal-field states of the Sm^{3+} multiplets under 20 000 cm^{-1} are given in Table I.

2. O_h center in CaF_2:0.05% Sm^{3+} and SrF_2:0.05% Sm^{3+} crystals

Centers of cubic symmetry are not normally observed in optical spectra, as the selection rules are restrictive due to the lack of an electric dipole moment. However, for Sm^{3+} the relevant optical absorption transition is $^6H_{5/2}\rightarrow{}^4G_{5/2}$ which satisfies the $\Delta J = 0$ magnetic dipole selection rule and transitions between these states for centers of cubic symmetry are observed.

Figures 5 and 6 show laser-excited selective fluorescence for O_h centers in CaF_2:Sm^{3+} and SrF_2:Sm^{3+} crystals. That the Sm^{3+} ions are in centers of cubic symmetry is confirmed by their simple energy-level structure and the lack of polarization dependence to the fluorescence in either (111)- or (100)-oriented crystals. As has been observed previously,[32]

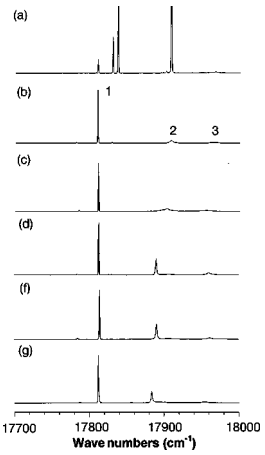

FIG. 9. (a) 16-K, $^4G_{5/2}$ excitation spectra for CaF_2:0.15%La^{3+}:0.05% Sm^{3+} monitoring all fluorescence in zero order of diffraction. 16-K, $^4G_{3/2}$ selective excitation for the Q centers in (b) CaF_2:0.15% La^{3+}:0.05% Sm^{3+} monitoring at 15 601 cm^{-1}, (c) CaF_2:0.15% Ce^{3+}:0.05% Sm^{3+} monitoring at 15 607 cm^{-1}, (d) CaF_2:0.15% Eu^{3+}:0.05% Sm^{3+} monitoring at 16 934 cm^{-1}, (e) CaF_2:0.15% Gd^{3+}:0.05% Sm^{3+} monitoring at 15 614 cm^{-1}, (f) CaF_2:0.15% Tb^{3+}:0.05% Sm^{3+} monitoring at 15 620 cm^{-1}.

TABLE II. 16-K calculated and experimental crystal-field energy levels of the O_h centers in CaF_2:Sm^{3+} and SrF_2:Sm^{3+} (as measured in air, ± 1 cm^{-1}). The value in round brackets is tentatively assigned, and has not been included in the fit.

Multiplet	State and Symmetry	CaF_2:Sm^{3+} Calc	CaF_2:Sm^{3+} Expt	SrF_2:Sm^{3+} Calc	SrF_2:Sm^{3+} Expt
$^6H_{5/2}$	$Z_1(\Gamma_8)$	−8	0	0	0
	$Z_2(\Gamma_7)$	102	96	115	93
$^6H_{7/2}$	$Y_1(\Gamma_6)$	910	(930)	944	955
	$Y_2(\Gamma_7)$	1143	1130	1104	1093
	$Y_3(\Gamma_8)$	1305	1314	1265	1284
$^6H_{9/2}$	$X_1(\Gamma_6)$	2150	2163	2175	2185
	$X_2(\Gamma_8)$	2339	2331	2309	2333
	$X_3(\Gamma_8)$	2511	2523	2469	-
$^6H_{11/2}$	$W_1(\Gamma_8)$	3510	3512	3518	3520
	$W_2(\Gamma_8)$	3745	3731	3708	3705
	$W_3(\Gamma_6)$	3753	-	3718	3714
	$W_4(\Gamma_7)$	3887	-	3830	3830
$^6H_{13/2}$	$V_1(\Gamma_8)$	4849	4849	4870	4872
	$V_2(\Gamma_7)$	4980	4967	4968	4967
	$V_3(\Gamma_8)$	5207	5213	5168	5146
	$V_4(\Gamma_7)$	5229	5237	5174	5161
	$V_5(\Gamma_6)$	5273	-	5218	5192
$^6H_{15/2}$, $^6F_{1/2}$ and $^6F_{13/2}$	$S_1(\Gamma_8)$	6157	6154	1677	6176
	$S_2(\Gamma_6)$	6262	6258	6269	-
	$S_3(\Gamma_6)$	6566	-	6527	-
	$S_4(\Gamma_8)$	6725	6714	6689	6682
	$S_5(\Gamma_8)$	6758	6736	6703	6718
	$S_6(\Gamma_7)$	6855	6894	6784	6817
	$S_7(\Gamma_8)$	6927	6914	6852	6848
$^6F_{5/2}$	$R_1(\Gamma_7)$	7245	7260	7215	7227
	$R_2(\Gamma_8)$	7381	7362	7334	7316
$^6F_{7/2}$	$Q_1(\Gamma_7)$	8119	8117	8087	8087
	$Q_2(\Gamma_8)$	8129	8144	8106	8109
	$Q_3(\Gamma_6)$	8275	-	8234	-
$^4G_{5/2}$	$A_1(\Gamma_7)$	17 665	17 653	17 713	17 699
	$A_2(\Gamma_8)$	18 041	18 053	18 057	18 070
$^4F_{3/2}$	$B_1(\Gamma_8)$	18 841	18 842	18 871	18 871

the cubic center in CaF_2 crystals is present in significantly greater concentrations than in SrF_2 crystals. This is attributed to the greater degree of defect clustering in the CaF_2 host. It has been asserted[30] and recently proven,[28,29] that clustering in the fluorites is anion excess. Thus, as the extent to which clusters dominate the defect distribution increases, there is an associated increase in the cubic center concentration.

For laser excitation of either the $Z_1 \rightarrow A_1$ or A_2 transitions of the cubic center in CaF_2:Sm^{3+} and SrF_2:Sm^{3+}, 23 and 25 transitions, respectively, can be observed between Sm^{3+} electronic states (Figs. 5 and 6). Table II gives the crystal-field energy-level assignments. The selection rules for rare-earth ions in centers of cubic symmetry allow magnetic di-

TABLE III. 16-K state energies (in air cm^{-1}, ± 1 unless otherwise stated) and polarization ratios (PR) of the $C_{3v}(O^{2-})$ centers in CaF_2:Sm^{3+} and SrF_2:Sm^{3+}.

Multiplet	Label	State energy	PR ZX/ZY	State energy	PR ZX/ZY
$^6H_{5/2}$	Z_1	0	1.3	0	1.1
	Z_2	35	1.1	45	0.7
	Z_3	421	1.3	477	0.8
$^6H_{7/2}$	Y_1	957	1.1	969	0.9
	Y_2	1322	0.9	1294	0.9
	Y_3	1432	1.4	1449	0.9
	Y_4	1515	1.3	1527	1.1
$^6H_{9/2}$	X_1	2001	1.2	1989	1.2
	X_2	2166	1.0	2176	1.1
	X_3	2401	0.7	2380	1.1
	X_4	2587	1.5	2582	1.1
	X_5	2689	0.7	2710	1.1
$^6H_{11/2}$	W_1	3467	0.9	3481	1.2
	W_2	3611	0.7	3612	1.2
	W_3	3840	1.1	3606	1.3
	W_4	3921	1.2	3941	1.2
	W_5	4043	-	3980	1.1
	W_6	4117	1.4	4135	0.8
$^6H_{13/2}$	V_1	4854	1.0	4872	1.1
	V_2	4916	1.0	4934	1.1
	V_3	5063	1.3	5049	-
	V_4	5274	-	5199	-
	V_5	5380	-	5247	-
	V_6	5490	-	5420	-
	V_7	5734	1.3	5758	1.3
$^6H_{15/2}$, $^6F_{1/2}$, $^6F_{3/2}$, and $^6F_{5/2}$	S_1	6184	1.0	6222	0.7
	S_2	6304	0.8	6337	0.9
	S_3	6338	0.9	6363	0.9
	S_4	6515	0.7	6479	0.6
	S_5	6601	1.1	6514	0.6
	S_6	6869	1.0	6575	0.8
	S_7	6890	1.0	6840	0.9
	S_8	7342	0.9	6869	1.0
	S_9	7394	1.4	7316	0.8
	S_{10}	7562	0.7	7356	1.0
	S_{11}	-	-	7365	1.1
	S_{12}	-	-	7533	0.7
	S_{13}	-	-	7569	0.8
$^6F_{7/2}$	Q_1	8151	1.6	8130	0.9
	Q_2	8233	1.0	8226	0.7
	Q_3	8242	0.9	8232	0.7
	Q_4	8323	1.0	8303	0.6
$^4G_{5/2}$	A_1	17 511	-	17 544	-
	A_2	18 095	-	18 126	-
	A_3	-	-	-	-
$^4F_{3/2}$	B_1	18 867	-	18 899	-
	B_2	18 981	-	19 032	-

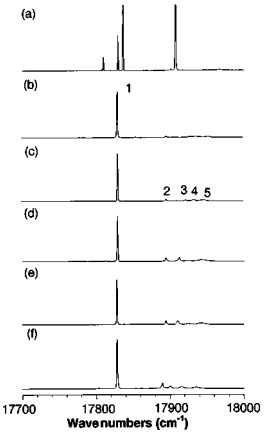

FIG. 10. (a) 16-K, $^4G_{5/2}$ excitation spectra for CaF_2:0.15% La^{3+}:0.05% Sm^{3+} monitoring all fluorescence in zero order of diffraction. 16 K, $^4G_{5/2}$ selective excitation for the *R* centers in (b) CaF_2:0.15% La^{3+}:0.05% Sm^{3+} monitoring at 15 613 cm^{-1}, (c) CaF_2:0.15% Ce^{3+}:0.05% Sm^{3+} monitoring at 15 617 cm^{-1}, (d) CaF_2:0.15% Eu^{3+}:0.05% Sm^{3+} monitoring at 16 942 cm^{-1}, (e) CaF_2:0.15% Gd^{3+}:0.05% Sm^{3+} monitoring at 15 628 cm^{-1} and (f) CaF_2:0.15% Tb^{3+}:0.05% Sm^{3+} monitoring at 15 637 cm^{-1}.

TABLE IV. 16-K excitation frequencies the $^4G_{5/2}$ multiplet of the CaF_2:0.15%R^{3+}:0.05% Sm^{3+} (where *R* = La, Ca, Eu, Gd, and Tb) *Q* and *R* centers. All frequencies are in air cm^{-1} (±1).

Center	State	La:Sm	Ce:Sm	Eu:Sm	Gd:Sm	Tb:Sm
Q	A_1	17 810	17 811	17 813	17 813	17 812
	A_2	17 905	17 900	17 887	17 885	17 881
	A_3	17 965	17 956	17 960	17 957	17 954
R	A_1	17 830	17 830	17 829	17 828	17 828
	A_2	17 894	17 893	17 891	17 889	17 888
	A_3	17 928	17 920	17 908	17 906	17 898
	A_4	17 938	17 931	17 922	17 918	17 913
	A_5	17 953	17 947	17 942	17 941	17 935

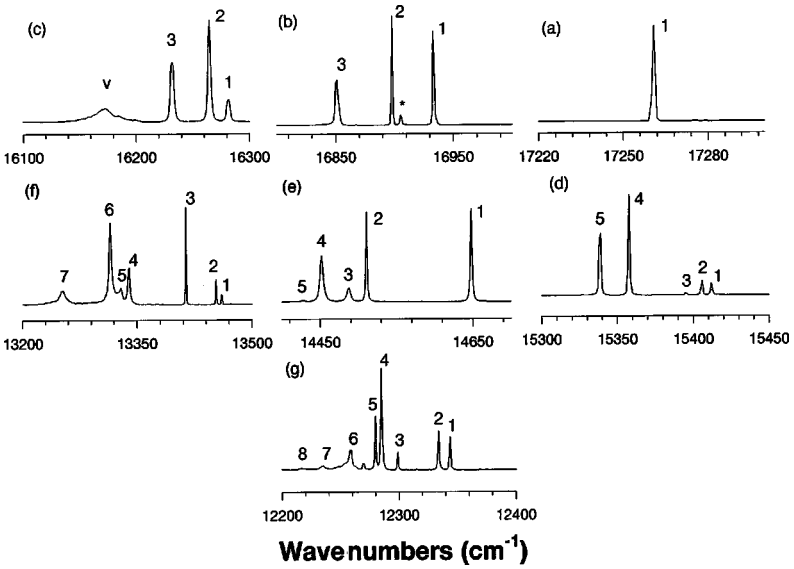

FIG. 11. 16-K fluorescence spectra for $Eu^{3+}(^5D_0)$ to (a) $^7F_0$, (b) $^7F_1$, (c) $^7F_2$, (d) $^7F_3$, (e) $^7F_4$,(f) $^7F_5$, and (e) $^7F_6$ of the heterogeneous *Q* center in CaF_2:0.15% Eu^{3+}:0.05% Sm^{3+}, *v* indicates a vibronic sideband, and the * notation an unrelated transition.

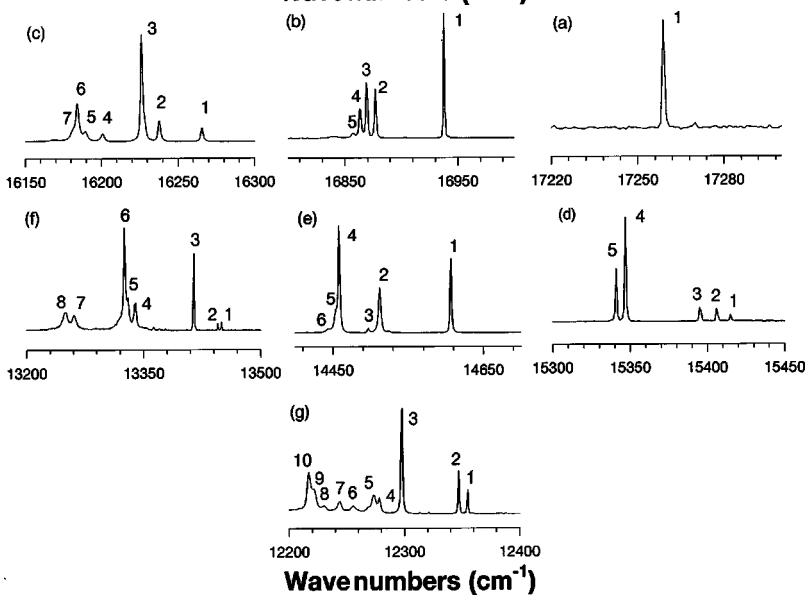

FIG. 12. 16-K fluorescence spectra for $Eu^{3+}(^5D_0)$ to (a) $^7F_0$, (b) $^7F_1$, (c) $^7F_2$, (d) $^7F_3$, (e) $^7F_4$, (f) $^7F_5$, and (e) $^7F_6$ of the heterogeneous *R* center in CaF_2:0.15% Eu^{3+}:0.05% Sm^{3+}. *v* indicates a vibronic sideband, and the * notation an unrelated transition.

TABLE V. 16-K $^5D_0 \rightarrow {}^7F_J$ state energies (as measured in air $cm^{-1} \pm 1$) for the Q(Eu, Sm) and R(Eu, Sm) centers in CaF_2:0.15% Eu^{3+}:0.05% Sm^{3+}.

Multiplet	State	Q(Eu, Sm)	R(Eu, Sm)
$^7F_0$	Z_1	0	0
$^7F_1$	Y_1	325	319
	Y_2	354	377
	Y_3	364	384
	Y_4	-	391
	Y_5	-	398
$^7F_2$	X_1	977	996
	X_2	994	1023
	X_3	1027	1034
	X_4	-	1060
	X_5	-	1071
	X_6	-	1077
	X_7	-	1093
$^7F_3$	W_1	1847	1845
	W_2	1853	1854
	W_3	1863	1865
	W_4	1901	1914
	W_5	1920	1920
$^7F_4$	V_1	2610	2654
	V_2	2749	2748
	V_3	2771	2764
	V_4	2806	2802
	V_5	2830	2804
	V_6	-	2815
$^7F_6$	U_1	3797	3811
	U_2	3805	3815
	U_3	3844	3846
	U_4	3918	3921
	U_5	3929	3931
	U_6	3943	3935
	U_7	4005	4000
	U_8	-	4011
$^7F_6$	T_1	4912	4906
	T_2	4924	4913
	T_3	4958	4963
	T_4	4973	4983
	T_5	4978	4987
	T_6	5001	5005
	T_7	5025	5017
	T_8	5040	5031
	T_9	-	5039
	T_{10}	-	5043

pole transitions between crystal-field states transforming as Γ_6, Γ_7, and Γ_8 irreps of the O_h double group except $\Gamma_6 \leftrightarrow \Gamma_7$. However, as can be seen in Table II, such transitions do occur (albeit weakly) possibly because the nonlocal charge compensation provides a weak axial distortion. Associated with zero-phonon transitions are transitions that terminate on vibronic states of the lattice. These phonon modes have strikingly narrow linewidths, and have been associated with resonant modes of the R^{3+} defect.[36]

Laser-excited fluorescence places the SrF_2:Sm^{3+} $^6H_{7/2}Y_1(\Gamma_6)$ state for the O_h center at 955 cm^{-1}, however, no corresponding feature is observed for the CaF_2:Sm^{3+} O_h center. From the observed vibronic structure we can tentatively place this state at 930 cm^{-1} [see Fig. 6(b)]. This value is consistent with the predictions of a crystal-field fit to all other levels that place it at 910 cm^{-1} (see Sec. VII).

3. $C_{3v}(O^{2-})$ center in CaF_2:0.05% Sm^{3+} and SrF_2:0.05% Sm^{3+} crystals

For CaF_2:Sm^{3+} and SrF_2:Sm^{3+} crystals treated in an atmosphere of dry oxygen gas, an additional center is observed. Oxygen charge compensated centers have been observed previously in both CaF_2:Sm^{3+} and SrF_2:Sm^{3+} crystals by EPR techniques[16,17] and also in optical experiments.[18,20,37,38] However in previous studies the oxygen was generally introduced as an unintentional impurity. In this study, the deliberate and controlled addition of oxygen allows the O^{2-} charge-compensated centers to be introduced and isolated without undue complication of the spectrum resulting from multiple O^{2-} charge-compensating configurations. The recorded fluorescence spectra of these centers is shown in Figs. 7 and 8.

The O^{2-} charge-compensated centers observed here are characterized by a large axial distortion. This would tend to support the assertion that the most commonly observed position for the O^{2-} ion is the nearest-neighbor substitutional position along the (111) direction from the R^{3+} ion. This results in a center of C_{3v} symmetry. Polarization of the 39 and 42 fluorescence transitions observed for the O^{2-} centers in CaF_2:Sm^{3+} and SrF_2:Sm^{3+}, respectively, show only a weak polarization dependence for (111)-oriented crystals, and no effect for (100)-oriented crystals (Table III). This is consistent with a trigonal symmetry center.

IV. SPECTROSCOPY OF CLUSTER CENTERS IN CaF_2:0.15% R^{3+}:0.05% Sm^{3+}; R^{3+}=La^{3+}, Ce^{3+}, Eu^{3+}, Gd^{3+} AND Tb^{3+}

Laser-selective excitation studies of CaF_2:Eu^{3+} have shown the presence of anion excess dimer (R) and trimer (Q) centers.[4,23,28,29,31,34] The R center has been shown to consist of two R^{3+} ions and three F^- ions arranged such that the two R^{3+} ions experience dissimilar crystal fields while the Q center is a symmetric cluster of three R^{3+} ions with four F^- ions. Analogous centers are present in CaF_2:Sm^{3+} ions, which, in this case, do not fluoresce due to efficient energy-transfer cross relaxation. It has been established that these Sm^{3+} centers are the principal electron traps for photoionized Sm^{2+} ions in moderately doped samples[39,40] for which both the divalent and trivalent species are present. Thus they play an important role in persistent spectral holeburning of CaF_2:Sm^{2+}/Sm^{3+}, where the holeburning mechanism is photoionization of the Sm^{2+} ions.[10]

As the homogeneous Sm^{3+} clusters do not fluorescence, the energy-level structure of these centers cannot be readily obtained using laser-selective excitation. Here, we have codoped the parent CaF_2:Sm^{3+} crystals with additional R^{3+}

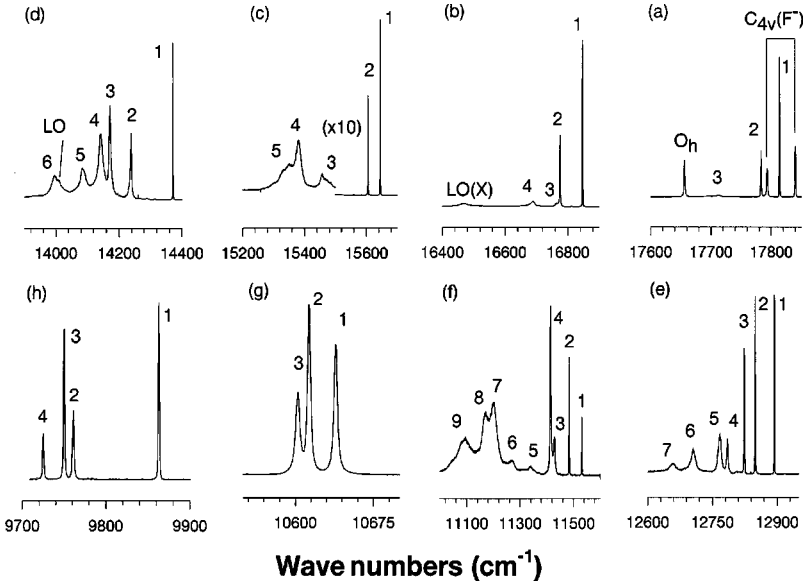

FIG. 13. 16-K unpolarized fluorescence spectra from $Sm^{3+}(^4G_{5/2})$ to the (a) $^6H_{5/2}$, (b) $^6H_{7/2}$, (c) $^6H_{9/2}$, (d) $^6H_{11/2}$, (e) $^6H_{13/2}$, (f) $^6F_{3/2}$, (g) $^6F_{5/2}$, and (h) $^6F_{7/2}$ multiplets of the heterogeneous Q center in CaF_2:0.15% La^{3+}:0.05% Sm^{3+} crystals.

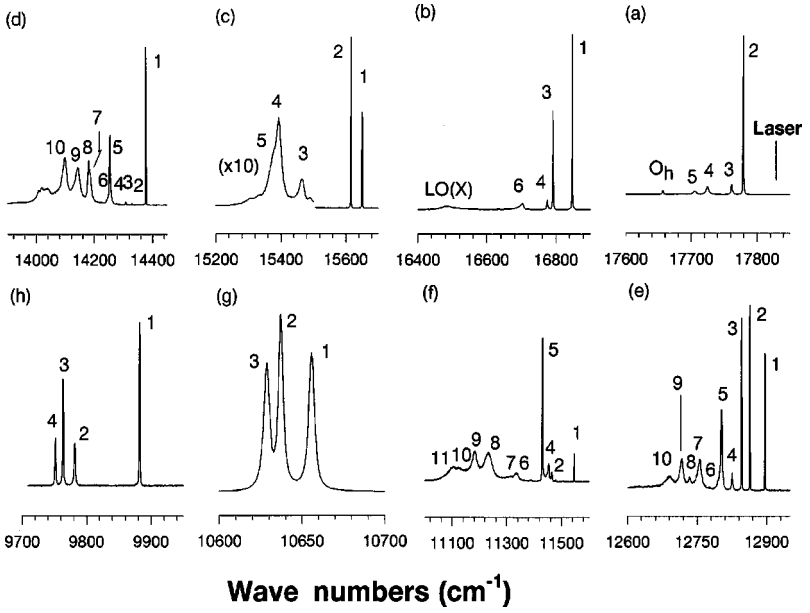

FIG. 14. 16-K unpolarized fluorescence spectra from $Sm^{3+}(^4G_{5/2})$ to the (a) $^6H_{5/2}$, (b) $^6H_{7/2}$, (c) $^6H_{9/2}$, (d) $^6H_{11/2}$, (e) $^6H_{13/2}$, (f) $^6H_{15/2}$, $^6F_{1/2}$, and $^6F_{3/2}$, (g) $^6F_{5/2}$, and (h) $^6F_{7/2}$ multiplets of the heterogeneous R center in CaF_2:0.15% La^{3+}:0.05% Sm^{3+} crystals.

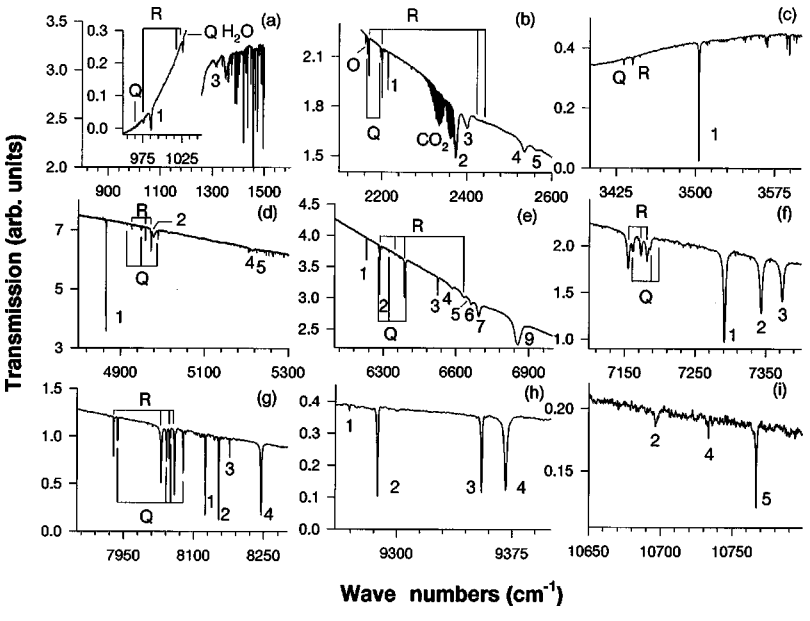

FIG. 15. 10-K infrared-absorption spectra for transitions to (a) $^6H_{7/2}$, (b) $^6H_{9/2}$, (c) $^6H_{11/2}$, (d) $^6H_{13/2}$, (e) $^6H_{15/2}$, $^6F_{1/2}$, and $^6F_{3/2}$, (f) $^6F_{5/2}$, (g) $^6F_{7/2}$, (h) $^6F_{9/2}$, and (i) $^6F_{11/2}$ multiplets in CaF_2:0.05% Sm^{3+}. The numerics indicate $C_{4v}(F^-)$ center transitions, while the Q and R centers are indicated with lines.

TABLE VI. 16-K state energies for the ^6H_J and ^6F_J multiplets of the heterogeneous Q centers in CaF_2:0.15% R^{3+}:0.05% Sm^{3+} where $R^{3+}=La^{3+}$, Ce^{3+}, Gd^{3+}, and Tb^{3+}. All energies are as measured in air ($cm^{-1}\pm1$).

Multiplet	State	La:Sm	Ce:Sm	Gd:Sm	Tb:Sm
$^6H_{5/2}$	Z_1	0	0	0	0
	Z_2	30	29	31	26
	Z_3	102	90	80	73
$^6H_{7/2}$	Y_1	968	966	966	964
	Y_2	1039	1034	1031	1025
	Y_3	1050	1053	-	-
	Y_4	1126	1120	1111	1111
$^6H_{9/2}$	X_1	2169	2167	2167	2163
	X_2	2209	2204	2198	2191
	X_3	2355	2350	2346	2342
	X_4	2431	2428	2426	2420
	X_5	2460	2463	2465	2461
$^6H_{11/2}$	W_1	3442	3438	3433	3428
	W_2	3575	3574	3574	3572
	W_3	3642	3638	3635	3631
	W_4	3669	3670	3671	3671
	W_5	3726	3718	3710	3697
	W_6	3815	3808	3801	3808
$^6H_{13/2}$	V_1	4919	4917	4916	4914
	V_2	4964	4958	4950	4943
	V_3	4989	4987	4991	4990
	V_4	5028	5024	5026	5029
	V_5	5046	5044	5044	5037
	V_6	5105	5100	5098	5088
	V_7	5151	5144	5137	5130
$^6H_{15/2}$, $^6F_{1/2}$, and $^6F_{3/2}$	S_1	6281	6286	6284	6282
	S_2	6329	6330	6322	6318
	S_3	6384	6385	6370	-
	S_4	6399	6399	6393	6389
	S_5	6475	6475	6464	6456
	S_6	6543	6538	6530	6525
	S_7	6612	6612	6612	6612
	S_8	6643	6642	6636	6628
	S_9	6721	6725	6729	6721
$^6F_{8/2}$	R_1	7168	7168	7163	7163
	R_2	7194	7193	7188	7187
	R_3	7205	7205	7201	7201
$^6F_{7/2}$	Q_1	7945	7943	7938	7935
	Q_2	8048	8045	8042	8043
	Q_3	8059	8056	8051	8050
	Q_4	8085	8082	8080	8076

ions to obtain heterogeneous cluster centers in order to promote detectable fluorescence from the modified R and Q centers. With the exception of Eu^{3+}, these ions were chosen for having suitable energy-level schemes such that no energy-transfer processes should be apparent. In the case of Eu^{3+} codoping, almost complete energy transfer from Sm^{3+} to

TABLE VII. 16-K state energies for the ^6H_J and ^6F_J multiplets of the heterogeneous R centers in CaF_2:0.15% R^{3+}:0.05% Sm^{3+} where $R^{3+}=La^{3+}$, Ce^{3+}, Gd^{3+}, and Tb^{3+}. All energies are as measured in air ($cm^{-1}\pm1$).

Multiplet	State	La:Sm	Ce:Sm	Gd:Sm	Tb:Sm
$^6H_{5/2}$	Z_1	0	0	0	0
	Z_2	54	$\frac{49}{52}$	37	22
	Z_3	72	70	67	68
	Z_4	109	103	82	98
	Z_5	127	123	106	-
$^6H_{7/2}$	Y_1	985	983	976	969
	Y_2	-	1022	1011	1010
	Y_3	1042	1037	1024	1018
	Y_4	1058	1155	1045	1037
	Y_5	-	1077	1067	1101
	Y_6	1132	1126	1107	1112
$^6H_{9/2}$	X_1	2180	2180	2169	2163
	X_2	2217	2213	2200	2191
	X_3	2367	2362	2347	2343
	X_4	2439	2434	2420	2415
	X_5	2453	2451	2444	2435
$^6H_{11/2}$	W_1	3456	3451	3440	3432
	W_2	3501	3491	-	-
	W_3	3525	3520	3512	3504
	W_4	3553	3547	3533	3525
	W_5	3579	3576	3568	3564
	W_6	-	3614	3599	-
	W_7	3649	3642	3633	3627
	W_8	3653	3648	3636	-
	W_9	3690	3686	3682	3676
	W_{10}	3734	3729	-	3698
$^6H_{13/2}$	V_1	4936	4934	4927	4923
	V_2	4969	4967	4959	$\frac{4950}{4951}$
	V_3	4987	4983	4973	4970
	V_4	5007	5005	4995	-
	V_5	5030	5023	5014	5008
	V_6	5033	5029	5026	5022
	V_7	5076	5072	5047	5041
	V_8	5097	5092	5080	-
	V_9	5114	5107	5087	5074
	V_{10}	5141	5134	5119	5112
$^6H_{15/2}$, $^6F_{1/2}$, and $^6F_{3/2}$	S_1	6287	6293	6286	6285
	S_2	6369	6370	6349	6341
	S_3	-	6380	6354	-
	S_4	6380	6388	6364	6359
	S_5	6405	6403	6388	6382
	S_6	6501	6499	6481	6475
	S_7	6514	6529	6501	6497
	S_8	6600	6595	6584	6582
	S_9	6653	6643	6628	6624
	S_{10}	6713	6704	6712	6711
	S_{11}	6728	6726	6729	6724
$^6F_{5/2}$	R_1	7173	7170	7155	7151
	R_2	7190	7188	7173	7167
	R_3	7199	7196	7181	7176
$^6F_{7/2}$	Q_1	7947	7942	7927	7924
	Q_2	8045	8043	8029	8027
	Q_3	8066	8061	8047	8044
	Q_4	8076	8072	8058	8056

TABLE VIII. 16-K $^4G_{5/2}A_1$ decay times (in milliseconds, ± 0.4) for the $C_{4v}(F^-)$, O_h and $C_{3v}(O^{2-})$ centers in CaF_2:Sm^{3+} and SrF_2:Sm^{3+} and for the heterogeneous R and Q centers in CaF_2:0.15% R^{3+}:0.05% Sm^{3+}; where $R^{3+}=La^{3+}$, Ce^{3+}, Eu^{3+}, Gd^{3+}, and Tb^{3+}. The CaF_2:0.15% Eu^{3+}:0.05% Sm^{3+}, $^4G_{5/2}$ lifetime is given in microseconds (± 0.3). The bracketed values are the homogeneous R and Q center values for CaF_2:0.1% Eu^{3+} measured in Ref. 4.

		Lifetime	
Center	Multiplet	CaF_2:Sm^{3+}	SrF_2:Sm^{3+}
$C_{4v}(F^-)$	$^4G_{5/2}$	10.4	10.5
O_h	$^4G_{5/2}$	26.3	22.5
$C_{3v}(O^{2-})$	$^4G_{5/2}$	6.3	5.3
Q(La, Sm)	$^4G_{5/2}$	7.8	
Q(Ce, Sm)	$^4G_{5/2}$	7.7	
Q(Eu, Sm)	$^4G_{5/2}$	3.4 μs	
Q(Eu, Sm)	$^5D_0$	8.4(10.1$\pm$0.1)	
Q(Gd, Sm)	$^4G_{5/2}$	7.7	
Q(Tb, Sm)	$^4G_{5/2}$	7.8$\pm$0.2	
R(La, Sm)	$^4G_{5/2}$	7.3	
R(Ce, Sm)	$^4G_{5/2}$	7.3	
R(Eu, Sm)	$^4G_{5/2}$	6.5 μs	
R(Eu, Sm)	$^5D_0$	10.5(10.4$\pm$0.1)	
R(Gd, Sm)	$^4G_{5/2}$	7.4	
R(Tb, Sm)	$^4G_{5/2}$	7.5$\pm$0.2	

Eu^{3+} is observed. The Eu^{3+} codoped samples also allow the unambiguous assignment of the Sm^{3+} centers to their CaF_2:Eu^{3+} analogs. In this case, the $^4G_{5/2}$ excitation spectra were recorded monitoring the $Eu^{3+}(^5D_0 \rightarrow {}^7F_1)$ fluorescence (via efficient phonon-assisted energy-transfer processes,[41]) while in all others cases the $Sm^{3+}(^4G_{5/2} \rightarrow {}^6H_{7/2})$ fluorescence was monitored. Figures 9 and 10 show the $^4G_{5/2}$ excitation spectra for the heterogeneous Q and R centers, respectively.

The measured transition frequencies show small shifts from those measured for the homogeneous Sm^{3+} clusters (Table IV). These $^4G_{5/2}$ multiplet splittings are generally consistent with the models proposed[28] for the Q and R centers in that only $J+1/2$ states can be detected for the R center as is appropriate for rare-earth ions experiencing identical electrostatic site potentials. By contrast, five $^4G_{5/2}$ states are detected for the R center due to the differing potentials experienced by the ions in that center.

For excitation of the Sm^{3+}, $^4G_{5/2}Z_1 \rightarrow A_1$ transition of either the R or Q center in CaF_2:0.15% Eu^{3+}:0.05% Sm^{3+} (at 17 813 and 17 829 cm^{-1}, respectively), efficient and complete energy transfer to the Eu^{3+5} D_0 state occurs.[41] Such Sm^{3+}-Eu^{3+} energy-transfer processes have been observed previously in doubly doped phosphate glass.[42] Figure 11 shows the Q-center Eu^{3+} fluorescence which bears a close similarity to the fluorescence of the homogeneous Q center in CaF_2:Eu^{3+}.[4] Figure 12 shows the heterogeneous R-center fluorescence for CaF_2:0.15% Eu^{3+}:0.05% Sm^{3+}. Table V gives the energy-level schemes of these centers. A broad feature at 16 837 cm^{-1} is assigned as a transition terminating on a pseudolocalized vibrational mode of the defect. The inferred vibrational frequency is 105 cm^{-1}, 9 cm^{-1} larger than that measured for the homogeneous R center in CaF_2:Eu^{3+}.[4] It is reasonable to assume that this effect is associated with the replacement of one of the Eu^{3+} ions with a lighter Sm^{3+} ion.

Doping CaF_2:Sm^{3+} with La^{3+}, Ce^{3+}, Gd^{3+} or Tb^{3+} yields heterogeneous clusters for which the Sm^{3+} ion fluoresces exclusively. This conveniently allows us to infer the energy levels of the analogous homogeneous Sm^{3+} centers which can be detected by optical and infrared absorption (Secs. III and VI). Representative fluorescence spectra are shown for the Q and R centers of CaF_2:0.15% La^{3+}:0.05% Sm^{3+} in Figs. 13 and 14, while the Sm^{3+} energy levels inferred for all four systems are given in Tables VI and VII. In both centers, fluorescence to the $^6H_{5/2}$ multiplet shows transitions to the $C_{4v}(F^-)$ and O_h centers as the vibrational sidebands of these centers overlap the Q and R center absorption transitions.

V. FLUORESCENCE LIFETIMES

The 16-K fluorescence lifetimes of the $^4G_{5/2}$ multiplet have been measured for the $C_{4v}(F^-)$, O_h and $C_{3v}(O^{2-})$

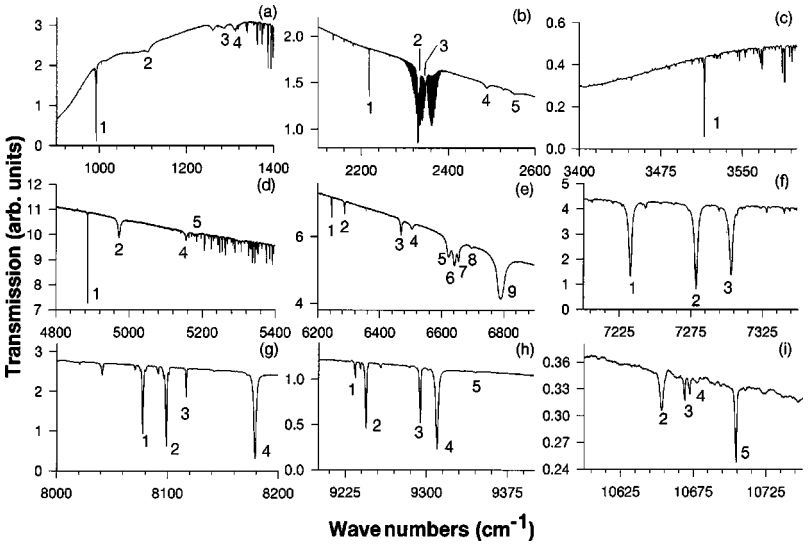

FIG. 16. 10-K infrared-absorption spectra for transitions to (a) $^6H_{7/2}$, (b) $^6H_{9/2}$, (c) $^6H_{11/2}$, (d) $^6H_{13/2}$, (e) $^6H_{15/2}$, $^6F_{1/2}$, and $^6F_{3/2}$, (f) $^6F_{5/2}$, (g) $^6F_{7/2}$, (h) $^6F_{9/2}$, and (i) $^6F_{11/2}$ multiplets in SrF_2:0.05% Sm^{3+}. The numerics indicate $C_{4v}(F^-)$ center transitions.

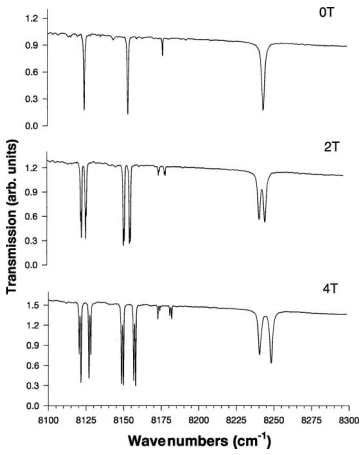

FIG. 17. Representative (111) Zeeman infrared spectra for transitions to the $^6F_{7/2}$ multiplet in CaF_2:0.05% Sm^{3+}.

centers in CaF_2:Sm^{3+} and SrF_2:Sm^{3+}, as well as the *Q*- and *R*-cluster centers in codoped CaF_2 crystals. The measured Sm^{3+} lifetimes (excepting that of the heterogenous clusters in CaF_2:0.15% Eu^{3+}:0.05% Sm^{3+}) presented in Table VIII are entirely radiative as the $^4G_{5/2}$–$^6F_{11/2}$ energy gap is 7500 cm^{-1}, assuming no interaction between the R^{3+} centers at the low concentrations used here. Therefore, the decay rates are determined only by the radiative transition probabilities. This is reflected in the measured decay rates with the O^{2-} charge-compensated centers having the shortest lifetimes

TABLE IX. Optimized free-ion and crystal-field parameters for the $C_{4v}(F^-)$ and O_h centers in CaF_2:Sm^{3+} and SrF_2:Sm^{3+}. Those in square brackets were not varied but were held at the values in Ref. 44.

	CaF_2:Sm^{3+}		SrF_2:Sm^{3+}	
Parameter	C_{4v}	O_h	C_{4v}	O_h
F^2	78 824	79 587	79 062	79 988
F^4	56 842	56 562	56 870	56 798
F^6	39 972	40 429	40 077	40 809
α	[21.6]	[21.6]	[21.6]	[21.6]
β	[−724]	[−724]	[−724]	[−724]
γ	[1700]	[1700]	[1700]	[1700]
T^2	[291]	[291]	[291]	[291]
T^3	[13]	[13]	[13]	[13]
T^4	[34]	[34]	[34]	[34]
T^6	[−193]	[−193]	[−193]	[−193]
T^7	[288]	[288]	[288]	[288]
T^8	[330]	[330]	[330]	[330]
M^{tot}	[2.4]	[2.4]	[2.4]	[2.4]
P^{tot}	[341]	[341]	[341]	[341]
ζ	1166	1174	1168	172
B_A^2	746	-	472	-
B_A^4	590	-	545	-
B_A^6	617	-	489	-
B_C^4	−1227	−2112	−1204	−1890
B_C^6	670	945	562	776
σ	11	16	13	16
n	49	26	53	28

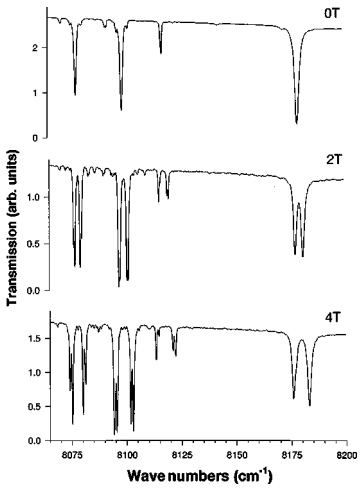

FIG. 18. Representative (111) Zeeman infrared spectra for transitions to the $^6F_{7/2}$ multiplet in SrF_2:0.05% Sm^{3+}.

arising from the large axial perturbation.

For the CaF_2:0.15% Eu^{3+}:0.05% Sm^{3+} *R* and *Q* centers, the $Sm^{3+}(^4G_{5/2})$ lifetime is determined by the energy transfer rates to the $Eu^{3+}(^5D_0)$ level of 294 and 154 ms^{-1} for the *Q* and *R* centers, respectively. It is notable that the heterogeneous *Q*-center energy transfer rate is faster and the $Eu^{3+}(^5D_0)$ lifetime shorter, than the corresponding values in the heterogeneous *R* center. Further to this, the heterogeneous *Q* center $Eu^{3+}(^5D_0)$ lifetime of 8.4 ± 0.1 ms is shorter than the homogeneous *Q*-center lifetime in CaF_2:Eu^{3+} (Ref. 4) (as shown in Table VIII). Both of these factors tend to indicate a reduced separation for the *Q*-center rare-earth ions compared to those of the *R* center.

VI. INFRARED AND ZEEMAN INFRARED ABSORPTION OF CaF_2:Sm^{3+} AND SrF_2:Sm^{3+}

Trivalent samarium has 11 multiplets in the 800–11000-cm^{-1} infrared-absorption region, $^6H_{7/2\text{-}15/2}$ and $^6F_{1/2\text{-}11/2}$, and Figs. 15 and 16 show the absorption transitions to these levels. The spectra recorded for CaF_2:0.05% Sm^{3+} are significantly more complicated than those shown for SrF_2:0.05% Sm^{3+} because of strong absorption transitions due to the *Q*- and *R*-cluster centers. The level assignments are made by comparison with laser-selected fluorescence transitions from the $^4G_{5/2}$ multiplet (Sec. III), and serve to confirm the inferred energy-level structures. The homogeneous Sm^{3+} *Q*- and *R*-center transitions are made by comparison with the codoped samples, and shifts of up to several wavenumbers are observed. Fluorescence transitions to the $^6F_{9/2}$ and $^6F_{11/2}$ multiplets could not be observed due to the limited range of the IR photomultipliers used. Infrared absorption has positively identified seven and nine of these levels for the $C_{4v}(F^-)$ centers in CaF_2:0.05% Sm^{3+} and SrF_2:0.05% Sm^{3+}, respectively (see Table I).

Zeeman infrared-absorption measurements were made on the C_{4v} symmetry centers with (111)-oriented crystals of CaF_2:0.05% Sm^{3+} and SrF_2:0.05% Sm^{3+}. For the magnetic field directed along the (111) crystallographic direction, all C_{4v} centers are magnetically equivalent, and the Sm^{3+} site

symmetry is reduced to C_1. In such a field, a spectral line splits into four components corresponding to the Zeeman splitting of the two doubly degenerate levels. Representative splittings are shown for the $^6H_{7/2}$ multiplet in Figs. 17 and 18 for $CaF_2:Sm^{3+}$ and $SrF_2:Sm^{3+}$ respectively. The small ground state $Z_1(\gamma_6)$ splitting of 1.1 cm^{-1} for $CaF_2:Sm^{3+}$, or 1.2 cm^{-1} for $SrF_2:Sm^{3+}$ at 4 T, is not resolved for the higher-lying levels within a multiplet because of the larger homogeneously broadened linewidths for these transitions. The measured Zeeman splitting factors are given in Table I alongside the calculated values from Sec. VII below.

VII. CRYSTAL- AND MAGNETIC-FIELD ANALYSIS OF $C_{4v}(F^-)$ AND O_h CENTERS

Crystal-field analyses have been carried out to assist in the determination of the symmetry of the energy eigenstates and to obtain wave functions for the Zeeman analysis. The crystal-field Hamiltonians appropriate for O_h and C_{4v} symmetry, in terms of the Racah tensor operators[43], are of the form

$$H_{O_h}=B_C^4[C_0^{(4)}+\sqrt{5/14}(C_4^{(4)}+C_{-4}^{(4)})]+B_C^6[C_0^{(6)}-\sqrt{7/2}(C_4^{(6)}+C_{-4}^{(6)})],$$

$$H_{C_{4v}}=H_{O_h}+B_A^2C_0^{(2)}+B_A^4[C_0^{(4)}-\sqrt{7/10}(C_4^{(4)}+C_{-4}^4)]+B_A^6[C_0^{(6)}+\sqrt{1/14}(C_4^{(6)}+C_{-4}^{(6)})].$$

The chosen tensor combinations are the invariant scalars in the point group symmetry reduction chain $SO_3\rightarrow O\rightarrow D_4\rightarrow C_4$. The parameters of this Hamiltonian are linearly related to those used earlier[1] by the relationships

$$B_A^2=B_0^2,$$

$$B_A^4=\frac{5}{12}B_0^4,$$

$$B_A^6=\frac{7}{8}B_0^6,$$

$$B_C^4=B^4+\frac{7}{12}B_0^4,$$

$$B_C^6=B^6+\frac{1}{8}B_0^6.$$

The crystal-field fitting routine using this Hamiltonian was supplied by Dr Mike Reid. For the Zeeman analyses the combined crystal- and magnetic-field perturbation matrices were simultaneously diagonalized with the addition of the Zeeman interaction term

$$H_{\text{Zeeman}}=\mu_B(\mathbf{L}+2\mathbf{S})\cdot\mathbf{B},$$

where $\mu_B=0.4669\ cm^{-1}/T$ is the Bohr magneton. The magnetic splitting factor s of a given Zeeman split level is defined in terms of its splitting ΔE in a magnetic field $\mathbf{B}$ by $s=\Delta E/\mu_B B$. For magnetic fields applied along the (111) directions of C_{4v} symmetry centers, the magnetic splitting factor is $s_{(111)}$, which is related to the parallel and perpendicular splitting factors $s_\parallel$ and $s_\perp$ by

$$3s_{(111)}^2=s_\parallel^2+2s_\perp^2.$$

Crystal-field fits to 49 and 53 energy levels of the $C_{4v}(F^-)$ centers and 26 and 28 energy levels of the O_h centers in $CaF_2:Sm^{3+}$ and $SrF_2:Sm^{3+}$ were performed using the combined results of the laser-selective excitation measurements and infrared absorption measurements (see Tables I and II). In these calculations, the f^5 configuration was truncated to the lowest 250 electronic levels as a reasonable approximation to the entire configuration. For the C_{4v} symmetry centers nine free parameters were employed in the fits to obtain standard deviations of 11 and 13 cm^{-1} for the CaF_2 and SrF_2 hosts, respectively. The optimized crystal-field parameters, shown in Table IX, compare well with the results of previous crystal-field fits for other rare-earth ions.[1,3,6,7,13]

Analysis of the optimised crystal-field wave functions shows considerable J mixing due to the crystal field. This accounts for the multipolar character of the emission from $^4G_{5/2}$ as most wave functions contain components which originate from states of $J=\frac{3}{2}$, $\frac{5}{2}$, or $\frac{7}{2}$. Thus emission of both electric and magnetic dipole characters is to be expected leading to degraded polarization behavior.[43,44]

The cubic center fits yield 16-cm^{-1} standard deviations in both cases, with crystal-field parameters that are close to one third larger than their C_{4v} symmetry counterparts. This decrease in the magnitude of the cubic field in the C_{4v} site can be attributed to a relaxation of the ligands in the cage around the R^{3+} in order to accommodate the F^- interstitial in the neighboring cage.[45] Within this, the magnitude of the cubic crystal-field parameters are perfectly reasonable, and the differences between these values and those of the C_{4v} symmetry centers may be attributed to the fact that the alkaline-earth fluoride lattices are overpacked.

Table I gives the calculated and measured (111) Zeeman splitting factors for the C_{4v} symmetry centers in CaF_2 and SrF_2. In general, good agreement is obtained between theory and experiment. For the $P_1(\gamma_6)$ and $P_2(\gamma_6)$ levels in CaF_2, second-order Zeeman effects have been neglected as the crystal-field splitting of these states is poorly accounted for by the fitting program. As a consequence of this, the program overestimates the second-order Zeeman effect between these states. Good agreement between the measured and calculated splitting factors is obtained with just the first-order interaction (see Table I).

VIII. CONCLUSIONS

Optical absorption, and laser selective excitation and fluorescence has yielded energy-level schemes for six centers in $CaF_2:Sm^{3+}$ and $SrF_2:Sm^{3+}$ crystals. The defect center distribution that has been determined consists of the well-known $C_{4v}(F^-)$ center plus a nonlocally charge-compensated cubic center in both the CaF_2 and SrF_2 host crystals. After brief treatment in dry oxygen gas, an additional center is created. This center has trigonal symmetry due to a charge-compensating O^{2-} ion in the nearest-neighbor substitutional position along the (111) direction from the R^{3+} ion.

In $CaF_2:Sm^{3+}$, two additional centers are observed that do not fluoresce. As the energy gap below the excited $^4G_{5/2}$ multiplet is 7500 cm^{-1}, direct multiphonon processes will be negligible. Also, a greater number of electronic transitions

are observed than expected for a single Sm^{3+} ion. This suggests these features are associated with dimer and trimer centers, analogous to those observed in CaF_2:Eu^{3+}. The optical excitation can thus be destroyed by energy-transfer cross-relaxation between the Sm^{3+} ions that comprise the cluster. Codoping CaF_2:0.05% Sm^{3+} crystals with 0.15% of LaF_3, CeF_3, EuF_3, GdF_3 and TbF_3 yields heterogeneous clusters for which Sm^{3+} emission is observed other than in CaF_2:0.15% Eu^{3+}:0.05% Sm^{3+}. In this case, efficient and complete energy transfer from $Sm^{3+}(^4G_{5/2})$ to $Eu^{3+}(^5D_0)$ is observed.

Crystal-field analyses of the O_h and $C_{4v}(F^-)$ center energy levels give good comparison with other R^{3+} ions in these crystals. Magnetic-field calculations using wave functions derived from the crystal-field analyses, accurately account for magnetic splitting factors measured by Zeeman infrared-absorption measurements.

ACKNOWLEDGMENTS

This research has been supported by the University of Canterbury and the New Zealand Lotteries Board. The authors would like to thank Dr. Mike F. Reid of the University of Canterbury for supplying his crystal-field fitting programs and Dr. Glynn D. Jones for many informative discussions. In addition, we would also like to thank Dr. Steven P. Jamison for drawing our attention to the existence of cubic center resonance vibrational modes. Technical assistance has been provided by R. A. Ritchie, W. Smith, R. Culley, and C. Rowe.

*Author to whom correspondence should be addressed. Present address: FELIX Free Electron Laser Facility, FOM Institute for Plasma Physics ''Rijnhuizen,'' Edisonbaan 14, P.O. Box 1207, 3430 BE Nieuwegein, The Netherlands. Fax: +31-30-6031204. Electronic address: wells@huygens.rijnh.nl

[1] C. A. Freeth and G. D. Jones, J. Phys. C **15**, 6833 (1982).
[2] R. J. Reeves, G. D. Jones, and R. W. G. Syme, Phys. Rev. B **46**, 5939 (1992); B. M. Tissue and J. C. Wright, *ibid.* **36**, 9781 (1987).
[3] T. P. J. Han, G. D. Jones, and R. W. G. Syme, Phys. Rev. B **47**, 14 706 (1993).
[4] R. J. Hamers, J. R. Wietfeldt, and J. C. Wright, J. Chem. Phys. **77**, 683 (1982).
[5] G. D. Jones and K. M. Murdoch, J. Lumin. **60&61**, 131 (1993); K. M. Murdoch, G. D. Jones, and R. W. G. Syme, Phys. Rev. B **56**, 1254 (1997).
[6] M. Mujaji, G. D. Jones, and R. W. G. Syme, Phys. Rev. B **46**, 14 398 (1992); M. B. Seelbinder and J. C. Wright, *ibid.* **20**, 4308 (1979).
[7] N. J. Cockcroft, D. Thompson, G. D. Jones, and R. W. G. Syme, J. Chem. Phys. **86**, 521 (1987); D. R. Tallant and J. C. Wright, *ibid.* **63**, 2074 (1975).
[8] N. M. Strickland, Ph.D. thesis, University of Canterbury, 1997.
[9] N. J. Cockroft, G. D. Jones, and R. W. G. Syme, J. Chem. Phys. **92**, 2166 (1990); M. D. Kurz and J. C. Wright, J. Lumin. **15**, 169 (1977).
[10] R. M. Macfarlane and R. M. Shelby, Opt. Lett. **9**, 533 (1984).
[11] W. Kaiser, C. G. B. Garrett, and D. L. Wood, Phys. Rev. **123**, 766 (1961).
[12] D. L. Wood and W. Kaiser, Phys. Rev. **126**, 2079 (1962).
[13] W. Low, Phys. Rev. **134**, A1479 (1964).
[14] M. J. Weber and R. W. Bierig, Phys. Rev. **134**, A1492 (1964).
[15] A. A. Antipin, I. I. Kurkin, L. D. Livanova, L. Z. Potvorova, and L. Ya. Shekun, Sov. Phys. Tech. Phys. **11**, 821 (1966).
[16] H. W. Evans and S. D. McLaughlan, Phys. Lett. **23**, 638 (1966).
[17] R. C. Newman and R. J. Woodward, J. Phys. C **7**, L432 (1974).
[18] T. F. Ewanizky, P. J. Caplan, and J. R. Pastore, J. Chem. Phys. **43**, 4351 (1965); N. Rabbiner, Phys. Rev. **130**, 502 (1963).
[19] N. Rabbiner, J. Opt. Soc. Am. **57**, 1376 (1967).
[20] H. Nara and M. Schlesinger, Phys. Rev. B **3**, 58 (1971).
[21] C. R. A. Catlow, A. V. Chadwick, and J. Corish, Radio Electron. Eng. **75**, 61 (1983).
[22] J. C. Wright, J. Phys. (Paris) Colloq. **41**, C6–434 (1980).
[23] J. C. Wright and K. M. Cirillo-Penn, Radiat. Eff. Defects Solids **119–121**, 231 (1991).
[24] D. R. Tallant and J. C. Wright, J. Chem. Phys. **63**, 2074 (1974).
[25] D. R. Tallant, D. S. Moore, and J. C. Wright, J. Chem. Phys. **67**, 2897 (1977).
[26] D. S. Moore and J. C. Wright, J. Chem. Phys. **74**, 1626 (1981).
[27] N. Suarez, E. Laredo, M. Diaz, A. Bello, and M. Puma, Radiat. Eff. Defects Solids **119-121**, 225 (1991).
[28] K. M. Cirillo-Penn and J. C. Wright, Phys. Rev. B **41**, 10 799 (1990).
[29] K. M. Cirillo-Penn and J. C. Wright, J. Lumin. **48&49**, 505 (1991).
[30] P. P. Yaney, D. M. Schaeffer, and J. L. Wolf, Phys. Rev. B **11**, 2460 (1975).
[31] J. L. Hall and R. T. Schumacher, Phys. Rev. **127**, 1892 (1962).
[32] J. P. Jouart, M. Bouffard, G. Klein, and G. Mary, J. Lumin. **50**, 273 (1991).
[33] N. M. Strickland and G. D. Jones, Phys. Rev. B **56**, 10 916 (1997).
[34] L. R. Olsen, A. O. Wright, and J. C. Wright, Phys. Rev. B **53**, 14 135 (1996).
[35] T. Luxbacher, H. P. Fritzer, and C. D. Flint, J. Phys.: Condens. Matter **7**, 9683 (1995).
[36] S. P. Jamison, R. J. Reeves, P. P. Pavlichuk, and G. D. Jones, J. Lumin. (to be published).
[37] K. Muto and K. Awazu, J. Phys. Chem. Solids **29**, 1269 (1968).
[38] L. V. Krotova, V. V. Osiko, and V. T. Udovenchik, Sov. Phys. Solid State **7**, 181 (1965)].
[39] W. Beck, D. Ricard, and C. Flytzanis, Appl. Phys. Lett. **69**, 3197 (1996).
[40] W. Beck, V. V. Fedorov, D. Ricard, C. Flytzanis, and T. T. Basiev, J. Lumin. **79**, 241 (1998).
[41] J.-P. R. Wells, G. D. Jones, and R. J. Reeves, J. Lumin. **72-74**, 977 (1997).
[42] R. Reisfeld and L. Boehm, J. Solid State Chem. **4**, 417 (1972).
[43] B. G. Wybourne, *Spectroscopic Properties of Rare-Earths* (Interscience, New York, 1965).
[44] W. T. Carnall, H. Crosswhite and H. M. Crosswhite (unpublished).
[45] D. P. Burum, R. M. Shelby, and R. M. Macfarlane, Phys. Rev. B **25**, 3009 (1982).